MINIREVIEW

CrossMark
← click for updates

Directed self-assembly of inorganic nanoparticles at air/liquid interfaces

Juan J. Giner-Casares*[a] and Javier Reguera*[b,c,d]

Inorganic nanoparticles (NPs) appear as the forefront functional structure in nanotechnology. The preparation of functional materials based on inorganic NPs requires their assembly onto well-defined structures. Within this context, self-assembly at air-liquid interfaces is probably the best candidate for a universal procedure for active materials composed of assembled NPs. The detailed *in situ* mechanism of the lateral self-assembly and vertical organization of NPs at air-liquid interfaces is still unknown despite its extended use. The most common and promising methods for addressing this open issue are reviewed herein. The self-assembled films can be used *in situ* or further be transferred to solid substrates as the main constituents of novel functional materials. Plasmonic NPs at interfaces are highly interesting, given the broad range of applications of the plasmonic field, and will be discussed more in detail.

Introduction

The ever growing presence of nanoparticles (NPs) in many aspects of our life is an undeniable reality. NPs are found in daily-use products such as sunscreens, batteries, or kitchen benches with antibacterial properties, as well as in more sophisticated systems such as the industrial production of chemicals or as drug delivery systems for cancer treatments.[1] Most of these applications involve some kind of interface, solid–solid, solid–liquid, solid–air, liquid–liquid, or liquid–air. In biomedicine, for instance, NPs interact with interfaces such as cell membranes, blood vessels, the blood–brain-barrier, cancer tissue, and other biointerfaces.[2] In heterogeneous catalysis, NPs deposited on solids (solid–air or solid–liquid interfaces) or located at emulsion and foam interfaces (liquid–liquid and liquid–air interfaces) are extensively used.[3] Many more applications can be found in optics, such as flexible and self-healing mirrors,[4] anti-reflecting substrates,[5] plasmonic rulers,[6] or in biomolecule sensing.[7] Chemical sensing with direct surface-enhanced Raman spectroscopy (SERS) at the liquid–liquid and liquid–air interfaces has resulted in very low limits of detection and highly reproducible and reliable

measurements of molecules of very different solubility.[8] The performance of NPs strongly depends on how they are adsorbed at the interfaces and their equilibrium position, their lateral interaction with other NPs, and their 2D ordering. All these factors affect their optical, electronic, or magnetic properties. Therefore, a fine control of their interactions, and their relative positions in the Z axis (perpendicular to the interface, concerning the immersion properties) and in the XY axis (parallel to the interface, concerning the assembly properties) will help not only to improve enormously all the current applications but also to create new ones taking advantage of specific types of interactions. To achieve this control, the current technology requires new synthetic methods to produce the desired surface chemistry, morphology, and size of NPs, together with new methods to quantify their 2D assembly and vertical organization.

This review is focused on inorganic NPs and their interaction and assembly at the air–liquid interface being extensively used in a wide range of applications and in most cases an intermediate step before the transfer of nanoparticle assemblies to solid substrates. Special emphasis is made on optical properties as an example to show how NP properties are highly affected by their assembly and immersion at the interface. This review is divided into two main parts that describe the organization of NPs at the air–liquid interfaces. First, the vertical organization of NPs at interfaces, its relation with the contact angle and adsorption energies, and the new techniques developed to measure those parameters. Second, the 2D organization of NPs (self-assembly) at the interface, the formation of supracrystals, and their properties as plasmonic substrates. Finally some conclusions and an outlook on the use of NPs at interfaces are given.

[a]*Institute of Fine Chemistry and Nanochemistry, Department of Physical Chemistry and Applied Thermodynamics, University of Córdoba, Campus Universitario de Rabanales, 14014 Córdoba, Spain. E-mail: jjginer@uco.es*
[b]*CIC biomaGUNE, Paseo de Miramón 182, 20009 Donostia-San Sebastián, Spain. E-mail: jreguera@cicbiomagune.es*
[c]*Ikerbasque, Basque Foundation for Science, 48013 Bilbao, Spain*
[d]*Biomedical Research Networking Center in Bioengineering Biomaterials and Nanomedicine (CIBER-BBN), 50018 Aragon, Spain*

Vertical position of nanoparticles at interfaces: measurement of the contact angle

The quantification of how strongly NPs are adsorbed at interfaces (adsorption energy) is decisive in very diverse applications. In the case of Pickering emulsions, used as colloidal nanocapsules for many different purposes, a strong adsorption providing higher emulsion stability over time is highly desirable. On the contrary, a lower adsorption in biomedical applications could increase the nanoparticle lifetime in the blood stream improving drug release, or increasing the imaging window when they are used as contrast agents.

The adsorption energy depends on the nanoparticle size, shape, and its surface properties, being described by the contact angle of the nanoparticle.[9,10] Given a certain type of NP, its contact angle, is therefore the key parameter to determine the energy of adsorption, the immersion depth (*i.e.* the vertical position), and even the orientation in the case of non-spherical NPs.[11] All of these parameters have a direct effect on the properties of NPs. For instance, the available area of NPs exposed to one of the two media of the interface affects the catalytic or the sensing capabilities of the reagents or analytes dissolved in such a medium. Moreover, the intrinsic properties of NPs also change with the different characteristics of the two media comprising the interface.

In optics for example, the plasmonic properties of NPs are affected by their vertical position with respect to the interface due to the difference in the dielectric constant of the two media (for instance $\varepsilon_{air} = 1$, and $\varepsilon_{water} = 80$).[12] Yang *et al.* showed, using finite difference time domain calculations (FDTD), how the localized surface plasmon resonance (LSPR) absorption band of gold NPs changed considerably depending on the vertical position of the NP, see Fig. 1A.[13] This vertical position also changed the plasmonic modes and formation of hot-spots on the assemblies of NPs, see Fig. 1B. Plasmonic NP dimers with a SERS enhancement of 10^7–10^9 could be achieved with the right control of the wavelength of excitation and the nanoparticle position.

Several studies have appeared in the last few years attempting to control this vertical position to address optical applications. Wang *et al.* used reagents such as dodecanethiol and tetramethylammonium at an oil or water phase respectively to drag the gold NPs to the interface.[14] Booth *et al.*, on the other hand, used an electrochemical modulation for this control.[15] Lin *et al.* employed a gel trapping method after the assembly of NPs at the air–water interface to build a substrate with partially immersed nanorods. However, most of these methods are far from being optimized as they lack the crucial quantification of the contact angle of the partially immersed NPs.

The evaluation of the contact angle is therefore of chief importance to achieve more efficient applications or even giving rise to new ones. However, only recently novel tools to measure this contact angle in a reliable way have appeared. Traditionally, the NP contact angle was measured using
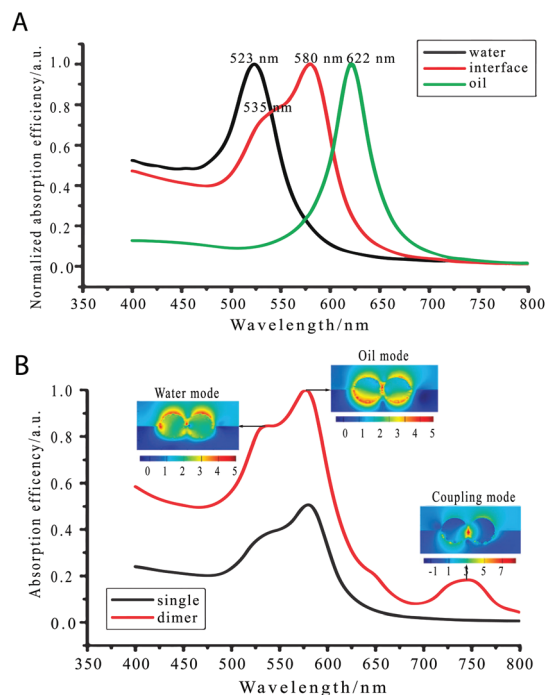

Fig. 1 (A) Calculated optical absorption spectra (far field) for a gold nanoparticle in water (black line), oil (green line), and at the water–oil interface (red line). (B) Calculated absorption spectra of gold nanoparticle dimers (red line) at the water–oil interface and the corresponding electric field distribution at three LSPR peaks.[13] Reproduced from ref. 13 with permission from the PCCP Owner Societies.

deposited NPs on a flat substrate, and placing a drop of water on top (sessile drop) to measure the contact angle at the triple interface line.[16,17]

However, measurements performed on these systems are influenced by the transfer process on the arrangement of NPs.[18,19] The following phenomena might take place during the transfer: dragging of NPs by the water droplet, chemical reactions of the cross-linkers added to fix NPs to the substrate, rearrangement of the NP capping ligands, low coverage and roughness on the substrate. Pinning and humidity are also major issues in contact angle measurement.[20] A lot of work is being done nowadays to develop techniques that allow the measurement of contact angles in a more accurate way. Two main groups are considered: trapping and masking techniques, and reflectivity measurements.

Evaluation of contact angles by trapping methods

One phase is solidified or gelified, allowing a later microscopy measurement. Individual NPs can be measured, being very interesting for not having uniform size or chemical surfaces. Note that the measurement is limited to few NPs, and the contact angle of very small NPs might be difficult to be assessed.

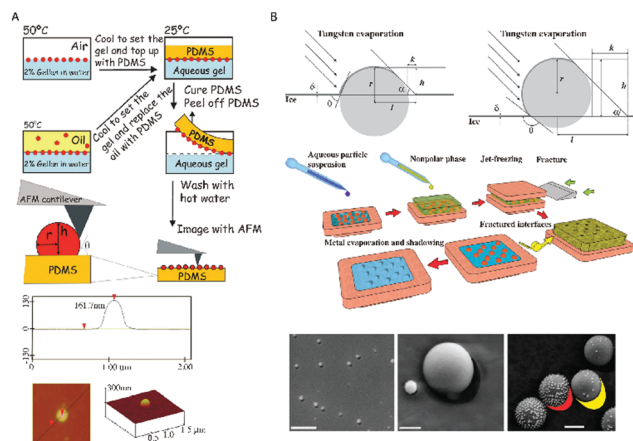Arnaudov *et al.* have used the Gel Trapping Technique (GTT) combined with atomic force microscopy (AFM) to

Fig. 2 Measurements of contact angles using trapping methods. (A) Gel trapping technique (GTT) combined with atomic force microscopy (AFM). The particle vertical position with respect to the PDMS interface is determined by AFM and it provides information about its three-phase contact angle at the liquid interface.[21] (B) Freeze-fracture shadow-casting cryo-scanning electron microscopy (FreSCa-cryoSEM). The three-phase contact angle, θ, is obtained geometrically by analysing the shadow after metal deposition with a defined angle.[23] Reproduced with permission from the PCCP Owner Societies, ref. 21, and Macmillan Publishers Ltd: *Nat. Commun.*[23] Copyright 2011.
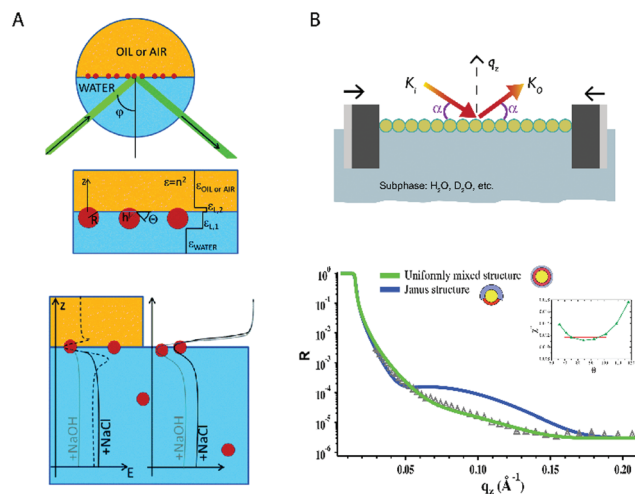

Fig. 3 Measurements of contact angles using reflectivity methods. (A) Ellipsometric method. The laser influenced from the bottom of the water–fluid interface where the NPs were adsorbed. The NPs were modeled as a two-layer system with average dielectric constants. The effect of ionic strength on the nanoparticle position was evaluated for MEO2MA-to-OEGMA covered NPs.[24] (B) Neutron reflectivity. Octanethiol–mercaptohexanol covered NPs were geometrically modelled using different ligand distributions (Janus and uniformly mixed). The equilibrium contact angle was obtained by minimizing the error of fitting χ^2.[25] Reproduced with permission from the PCCP Owner Societies, ref 24 and 25.

measure NPs as small as 37 nm in radius, see Fig. 2A.[21] NPs are trapped through a gelation process and then they are transferred to a PDMS matrix to be measured by a microscopy technique such as AFM[21] or SEM.[22]

A method based on freeze-fracture shadow-casting cryo-scanning electron microscopy (FreSCa-cryoSEM) has also been recently proposed, which allows measurements of contact angles of silica NPs with diameters higher than ten nanometers (Fig. 2B).[23] The aqueous phase is frozen and then an evaporated metal is deposited with a certain angle to generate a shadow that is measured with SEM. This method was used also at liquid–liquid interfaces with a fracture event before the measurement. By measuring the size of nanoparticles and the length of the shadow, the contact angle was geometrically obtained.

Evaluation of contact angles by reflectivity measurements

Reflectivity measurements offer vertical resolution, in principle up to the angstrom regime. A large number of NPs can be measured, in contrast to the microscopy methods discussed above. A high homogeneity in size, morphology, and surface composition of the NPs is required. Typically monolayers of NPs are measured. Ellipsometric measurements have been performed to obtain the contact angle of 18 nm metallic NPs covered by a stimuli-responsive polymeric shell. A two-layer model was used, see Fig. 3A. The contact angle was then calculated from the immersion depth assuming a spherical morphology.[24]

X-ray and neutron techniques provide a detailed picture of nanomaterials at interfaces.[26–29] X-ray reflectivity is the most used source to evaluate the contact angle of NPs at an interface.

Stefaniu *et al.* used X-ray reflectivity and infrared measurements to study the adsorption of polymer-coated gold NPs at interfaces.[30] The combination of both techniques indicates the conformation of the polymer and the adsorption and desorption processes. Calzolari *et al.* applied X-ray reflectivity to silica NPs at a water–hexane interface.[31] They determined the immersion depth and contact angles of the silica NP core in relation to different quantities of the surfactant cetyltrimethylammonium bromide dissolved in the aqueous media. Isa *et al.* expanded this work to address the influence of the NPs' shell architecture in determining the monolayer interfacial microstructure.[32] *In situ* high-energy X-ray reflectivity was used to quantify the vertical position and inter-particle spacing of core–shell iron oxide poly(ethylene glycol) (PEG) NPs adsorbed at water–*n*-decane interfaces. X-ray reflectivity measurements are highly interesting for plasmonic NPs, given the large contrast provided by their inorganic core. Other NPs or atom clusters containing electron rich atoms, such as polyoxometalates, can also be studied by reflectivity at the air-water interface.[33]

Note that soft materials with not enough contrast might be a limitation for this technique. Neutron reflectivity, on the other hand, can provide better contrast between different organic regions, expanding the X-ray reflectivity measurements to other kinds of NPs such as polymeric or hybrid inorganic–organic NPs. Additionally, neutron reflectivity allows the use of contrast variation, *i.e.* an isotopic change of one of the elements of the system keeping the same geometry, producing a different reflectivity profile.

Note that the much lower neutron flux of neutron beam instruments when compared with X-rays increases the measurement time, and the lower contrast for certain inorganic materials. Rezende *et al.* used neutron reflectivity to study the structural evolution of a Langmuir layer consisting of gold NPs grafted with thermosensitive poly(*N*-isopropyl acrylamide), with the structural changes induced by the polymer.[34] Ujihara *et al.* used neutron reflectivity to analyze the relative composition of a mixed Langmuir monolayer including gold NPs and amphiphilic poly(amido-amine) dendrimer molecules.[35]

Recently we have used neutron reflectivity for the first time to obtain the contact angle and adsorption energies of gold NPs covered by self-assembled monolayers.[25] In this work additional information was obtained with binary mixtures of ligands. Comparing the reflectivity results with different models we found that NPs covered by deuterated 1-octanethiol (OT) and 6-mercaptohexanol (MHol) tended to have a surface formed by a random distribution of the ligands or by small nanodomains. On the other hand, a Janus configuration did not produce an accurate fitting suggesting that it was highly improbable, see Fig. 3B. Furthermore, these results were validated with a contrast variation strategy. Changing the water subphase with different proportions of deuterated water provided several reflectivity profiles that were fitted into the same model validating and improving the measurement of the contact angle.

Lateral organization of nanoparticles

The air–liquid interface stands as a highly convenient platform for assembling NPs in a controlled manner, being experimentally simple and most versatile.[36] The group of Murray has spearheaded the assembly of inorganic NPs with a seminal publication on interface-assembled binary nanocrystals.[37] A fruitful series of protocols for assembling different inorganic NPs at air–liquid interfaces were subsequently developed, see Fig. 4.

These studies might be divided into two large categories of interfacial self-assembly. First, an application-driven design, *e.g.*, towards plasmonics (In-doped cadmium oxide NPs)[38] and photovoltaics (CuInSe$_2$ NPs).[39] Second, interfacial self-assembly based on the nanoparticle shape purposefully designed. This includes lanthanide fluoride planar NPs,[40] gadolinium NPs with complementary shape,[41] or binary supercrystals of NaYF$_4$ nanorods and F$_3$O$_4$ nanospheres, exploiting different shapes of NPs using alloys[42] and extended to even ternary supercrystals.[43]

Most of the above mentioned examples use the common procedure of hydrophobic NPs dispersed in hexane. The nanoparticle dispersion is spread on an air-diethylene glycol interface, with the monolayer of NPs readily obtained after the evaporation of hexane. This general procedure is being exploited by a large number of research groups worldwide, from which we highlight a recent study. Probably one of the
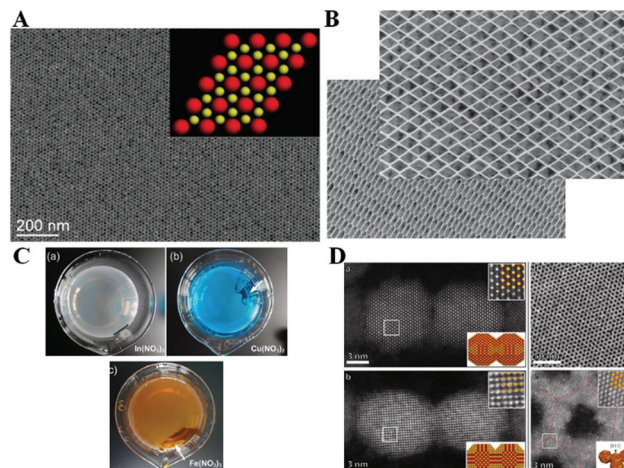

Fig. 4 (A) Binary nanocrystal superlattice as seminal achievement in assembling inorganic NPs at air-liquid interfaces by the group of Murray.[37] (B) DyF$_3$ rhombohedral nanoplates self-assembled in a parallel manner.[40] (C) Nb$_2$O$_5$ NPs at the air-liquid interface can selectively sense the presence of metal ions in bulk solution.[44] (D) The orientation of the attachment between PbSe NPs is determined by the facets in contact.[46] Reprinted with permission from Macmillan Publishers Ltd: *Nature*, ref. 37, copyright 2010 and *Nat. Chem.* copyright 2013; and from John Wiley and Sons: *Adv. Mater. Interfaces*, ref. 44, copyright 2015; and from ref. 46, copyright 2013 American Chemical Society.

most interesting aspects from this assembly procedure is the possibility of application to different compositions of NPs, such as Nb$_2$O$_5$ selectively responsive to ions in the bulk solution[44] or even binary assemblies of NaY/GdF$_4$.[45]

The orientation of NPs within the assemblies might even be controlled under certain conditions of facet contact, which is highly interesting as the idea of surface-homogeneous NPs coming together at the air–liquid interfaces might not be totally correct. Instead, a subtle effect as the facet design of the NPs might determine the overall assembly.[46] Another common strategy in interface science, as surfactant addition, can result in a remarkable selective self-assembly of anisotropic NPs, as an end-to-end contact of CdSe nanorods.[47] An unconventional study describes the formation of "drumheads" of a single monolayer of iron oxide NPs that displays mechanical resonance. Although free-standing membranes of NPs were previously achieved, this study paves the way for a new quantitative concept on their behavior.[48]

A newly developed protocol for assembling magnetic NPs onto ordered monolayers, in this case helical superstructures, has been reported by Klajn. The possibility of obtaining symmetry breaking, along with complex suprastructures from simple building blocks, will undoubtedly be highly useful in upcoming research.[50,51]

The lateral organization of NPs within a self-assembled monolayer is determined by a subtle balance of chemical compositions, morphology and size. A number of conditions are necessary for an optimal self-assembly onto an ordered monolayer. The NP should be chemically stable both when dissolved and exposed to air, *e.g.*, silver NPs tend to be quite stable in

solution but are readily reshaped when deposited on a substrate. The morphology might play a role when using complementary shapes, yet the shape of the core might not be relevant when using a thick coating layer. Concerning size, small NPs tend to be more easily assembled, although good assemblies might be obtained for larger NPs. The actual concern with the size of the NP would be polydispersity: the self-assembled NPs will segregate into domains of NPs with a similar size.

Self-assembly of plasmonic nanoparticles

The interfacial self-assembly of inorganic NPs finds an interesting niche in taking advantage of the collective plasmonic features of the assemblies. The main requirements of the assembly include a short interparticle distance to promote an effective plasmon coupling, as well as formation of large NP films in the macroscopic range.[49,52] The efforts devoted in this direction are manifold and mainly dedicated to improve the quality of the assembled films in terms of homogeneity and ordering. Probably one of the main open questions on the functionality of these plasmonic films is their mechanical and chemical endurance. Yet successful examples of functional plasmonic assemblies have been reported, effectively demonstrating that interfacial self-assembly is a useful option for obtaining functional plasmonic devices.[53]

Binary self-assembly of plasmonic NPs can be realized not only with different nanoparticle sizes as in previous examples of inorganic NPs, but also with different nanoparticle shapes. Indeed, Au nanowires can be co-assembled with Au NPs, guiding the assembly along the axis of the nanowire, see Fig. 5A.[54] This directed ordering might be of interest when anisotropic properties using plasmonics are pursued, as surface-enhanced spectroscopy using polarized light. Despite almost all of the published reports spread the NPs on top of a liquid surface and rely on spontaneous evaporation and self-assembly to achieve a close-packed monolayer, a mechanically induced packing of the NPs using the classical Langmuir trough might be highly beneficial. Stellacci *et al.* demonstrated the improvement of the assembled NP monolayer in a quite illustrative example. In this case, small and hydrophobic Au NPs functionalized with hydrophobic thiols were included. By applying moderate values of surface pressure in the range of 10–15 mN m^{-1} and with the use of mechanical annealing, the quality of the film in terms of homogeneity and long-range order (measured by pair-distribution function) became significantly better, see Fig. 5B.[54,55]

A traditional limitation of the interfacial assembling of plasmonic NPs is the size of the NPs. While large NPs are more interesting for plasmonic applications such as SERS, such NPs are more difficult to stabilize in organic solvents. This limitation can be partially overcome using functionalization with amphiphilic polymers, such as polyvinylpyrrolidone (PVP). Unfortunately the polymer-functionalized NPs are
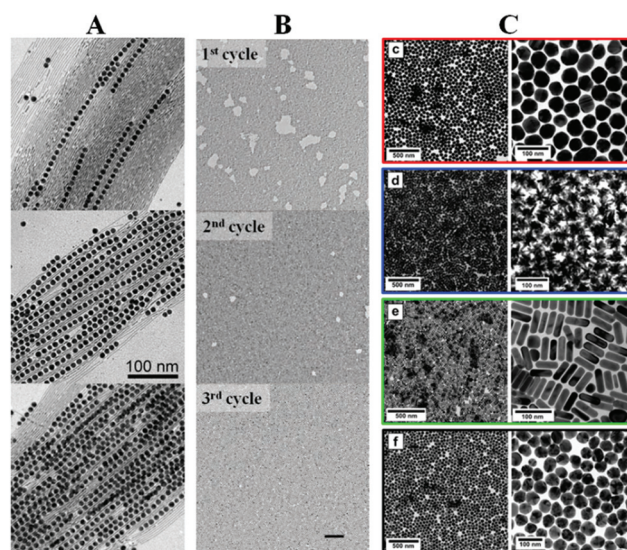

Fig. 5 (A) Au nanowires guide the self-assembly of smaller Au NPs.[51] (B) Langmuir technique can be used to improve the quality of the assembled films.[52] (C) An efficient protocol on phase transfer allows the subsequent interfacial self-assembly of a large variety of sizes and shapes of plasmonic NPs.[55] Reprinted with permission from John Wiley & Sons, Inc.: *Angew. Chem. Int. Ed.*,[51] copyright 2010; from John Wiley & Sons, Inc.: *Small*,[52] copyright 2011; from ref. 55. Copyright 2015 American Chemical Society.

not completely hydrophobic, thus hindering the dispersion in organic solvents. Moreover, an abundant amount of polymer is required for an efficient functionalization, which might prevent analytes or other molecules of interest from reaching the surface of the NPs. Even though plasmonic substrates have been successfully built by interfacial self-assembly of polymer-capped NPs, as published by our group in PVP-capped nanotriangles,[56] only recently this limitation has been overcome by using a combination of hydrophobic thiols and short PEG oligomers, accomplishing a complete phase transfer from an aqueous solution to an organic solvent without compromising the stability.[57] High quality monolayers composed of NPs with different sizes and shapes can be readily built using interfacial self-assembly, see Fig. 5C.

Conclusions

The self-assembly of inorganic NPs at air-liquid interfaces is already established as a versatile building technique, showing a recent burst of interest in the literature. The applications of the self-assembled NP films in different fields have stimulated such recent development, with plasmonics-based active films probably as the most remarkable purpose. Despite these efforts more work is still required to better understand the relationship among the structure, vertical position and orientation and lateral organization, and their properties. This is crucial to achieve more effective applications not only in

optics but also in other fields such as catalysis, magnetism and biomedicine.

The usual limitations for the efficient self-assembly of inorganic NPs arise mainly from their functionalization. Therefore an intensive effort is devoted from groups focused on chemistry, and surely new protocols will be developed in subsequent years. On the other hand, a common practical problem in the use of self-assembled films for plasmonic sensing is the presence of the functionalization agents that might interfere with molecules reaching the surface of NPs. The interplay between these two effects determines the general efficiency of the synthesis, assembly and application processes.

Acknowledgements

References

1 G. Schmid, *Nanoparticles: from theory to application*, WILEY-VCH Verlag, Weinheim, Germany, 2nd edn, 2011.

2 B. Pelaz, G. Charron, C. Pfeiffer, Y. Zhao, J. M. de la Fuente, X.-J. Liang, W. J. Parak and P. del Pino, *Small*, 2013, **9**, 1573–1584.

3 Y. Xia, H. Yang and C. T. Campbell, *Acc. Chem. Res.*, 2013, **46**, 1671–1672.

4 Y.-T. Yen, T.-Y. Lu, Y.-C. Lee, C.-C. Yu, Y.-C. Tsai, Y.-C. Tseng and H.-L. Chen, *ACS Appl. Mater. Interfaces*, 2014, **6**, 4292–4300.

5 H. Y. Koo, D. K. Yi, S. J. Yoo and D.-Y. Kim, *Adv. Mater.*, 2004, **16**, 274–277.

6 V. A. Turek, M. P. Cecchini, J. Paget, A. R. Kucernak, A. A. Kornyshev and J. B. Edel, *ACS Nano*, 2012, **6**, 7789–7799.

7 J. J. Giner-Casares, M. Henriksen-Lacey, M. Coronado-Puchau and L. M. Liz-Marzán, *Mater. Today*, 2016, **19**, 19–28.

8 M. P. Cecchini, V. A. Turek, J. Paget, A. A. Kornyshev and J. B. Edel, *Nat. Mater.*, 2012, **12**, 165–171.

9 P. Pieranski, *Phys. Rev. Lett.*, 1980, **45**, 569–572.

10 B. P. Binks, *Curr. Opin. Colloid Interface Sci.*, 2002, **7**, 21–41.

11 B. J. Park and D. Lee, *ACS Nano*, 2012, **6**, 782–790.

12 J. B. Edel, A. A. Kornyshev, A. R. Kucernak and M. Urbakh, *Chem. Soc. Rev.*, 2016, **45**, 1581–1596.

13 Z. Yang, S. Chen, P. Fang, B. Ren, H. H. Girault and Z. Tian, *Phys. Chem. Chem. Phys.*, 2013, **15**, 5374.

14 M. Wang, Z. Zhang and J. He, *Langmuir*, 2015, **31**, 12911–12919.

15 S. G. Booth, D. P. Cowcher, R. Goodacre and R. A. W. Dryfe, *Chem. Commun.*, 2014, **50**, 4482.

16 Y. Guo, D. Tang, Y. Du and B. Liu, *Langmuir*, 2013, **29**, 2849–2858.

17 P. M. Hansson, L. Skedung, P. M. Claesson, A. Swerin, J. Schoelkopf, P. A. C. Gane, M. W. Rutland and E. Thormann, *Langmuir*, 2011, **27**, 8153–8159.

18 R. Banerjee, M. K. Sanyal, M. K. Bera, A. Singh, J. Novak and O. Konovalov, *Phys. Rev. E: Stat., Nonlinear, Soft Matter Phys.*, 2011, **83**, 051605.

19 S. Kundu, K. Das and O. Konovalov, *AIP Adv.*, 2013, **3**, 092130.

20 J. N. Israelachvili, *Intermolecular and surface forces*, Academic Press, 3rd edn, 2011.

21 L. N. Arnaudov, O. J. Cayre, M. A. Cohen Stuart, S. D. Stoyanov and V. N. Paunov, *Phys. Chem. Chem. Phys.*, 2010, **12**, 328–331.

22 V. N. Paunov, *Langmuir*, 2003, **19**, 7970–7976.

23 L. Isa, F. Lucas, R. Wepf and E. Reimhult, *Nat. Commun.*, 2011, **2**, 438.

24 A. Stocco, G. Su, M. Nobili, M. In and D. Wang, *Soft Matter*, 2014, **10**, 6999–7007.

25 J. Reguera, E. Ponomarev, T. Geue, F. Stellacci, F. Bresme and M. Moglianetti, *Nanoscale*, 2015, **7**, 5665–5673.

26 B. T. Diroll, K. M. Weigandt, D. Jishkariani, M. Cargnello, R. J. Murphy, L. A. Hough, C. B. Murray and B. Donnio, *Nano Lett.*, 2015, **15**, 8008–8012.

27 K. Larson-Smith, A. Jackson and D. C. Pozzo, *Langmuir*, 2012, **28**, 2493–2501.

28 H. Jia, I. Grillo and S. Titmuss, *Langmuir*, 2010, **26**, 7482–7488.

29 M. Moglianetti, Q. K. Ong, J. Reguera, K. M. Harkness, M. Mameli, A. Radulescu, J. Kohlbrecher, C. Jud, D. I. Svergun and F. Stellacci, *Chem. Sci.*, 2014, **5**, 1232.

30 C. Stefaniu, M. Chanana, H. Ahrens, D. Wang, G. Brezesinski and H. Möhwald, *Soft Matter*, 2011, **7**, 4267.

31 D. C. E. Calzolari, D. Pontoni, M. Deutsch, H. Reichert and J. Daillant, *Soft Matter*, 2012, **8**, 11478.

32 L. Isa, D. C. E. Calzolari, D. Pontoni, T. Gillich, A. Nelson, R. Zirbs, A. Sánchez-Ferrer, R. Mezzenga and E. Reimhult, *Soft Matter*, 2013, **9**, 3789.

33 J. J. Giner-Casares, G. Brezesinski, H. Möhwald, S. Landsmann and S. Polarz, *J. Phys. Chem. Lett.*, 2012, **3**, 322–326.

34 C. A. Rezende, J. Shan, L.-T. Lee, G. Zalczer and H. Tenhu, *J. Phys. Chem. B*, 2009, **113**, 9786–9794.

35 M. Ujihara, K. Mitamura, N. Torikai and T. Imae, *Langmuir*, 2006, **22**, 3656–3661.

36 J. J. Giner-Casares, G. Brezesinski and H. Möhwald, *Curr. Opin. Colloid Interface Sci.*, 2014, **19**, 176–182.

37 A. Dong, J. Chen, P. M. Vora, J. M. Kikkawa and C. B. Murray, *Nature*, 2010, **466**, 474–477.

38 T. R. Gordon, T. Paik, D. R. Klein, G. V. Naik, H. Caglayan, A. Boltasseva and C. B. Murray, *Nano Lett.*, 2013, **13**, 2857–2863.

39 D. C. Reifsnyder, X. Ye, T. R. Gordon, C. Song and C. B. Murray, *ACS Nano*, 2013, **7**, 4307–4315.

40 X. Ye, J. Chen, M. Engel, J. A. Millan, W. Li, L. Qi, G. Xing, J. E. Collins, C. R. Kagan, J. Li, S. C. Glotzer and C. B. Murray, *Nat. Chem.*, 2013, **5**, 466–473.

41 T. Paik and C. B. Murray, *Nano Lett.*, 2013, **13**, 2952–2956.

42 X. Ye, J. A. Millan, M. Engel, J. Chen, B. T. Diroll, S. C. Glotzer and C. B. Murray, *Nano Lett.*, 2013, **13**, 4980–4988.

43 T. Paik, B. T. Diroll, C. R. Kagan and C. B. Murray, *J. Am. Chem. Soc.*, 2015, **137**, 6662–6669.

44 Z. Dai, H. Dai, Y. Zhou, D. Liu, G. Duan, W. Cai and Y. Li, *Adv. Mater. Interfaces*, 2015, **2**, 1500167.

45 T. Zheng, L.-D. Sun, J.-C. Zhou, W. Feng, C. Zhang and C.-H. Yan, *Chem. Commun.*, 2013, **49**, 5799.

46 W. H. Evers, B. Goris, S. Bals, M. Casavola, J. De Graaf, R. Van Roij, M. Dijkstra and D. Vanmaekelbergh, *Nano Lett.*, 2013, **13**, 2317–2323.

47 D. Kim, W. D. Kim, M. S. Kang, S.-H. Kim and D. C. Lee, *Nano Lett.*, 2015, **15**, 714–720.

48 P. Kanjanaboos, X.-M. Lin, J. E. Sader, S. M. Rupich, H. M. Jaeger and J. R. Guest, *Nano Lett.*, 2013, **13**, 2158–2162.

49 J. J. Giner-Casares and L. M. Liz-Marzán, *Nano Today*, 2014, **9**, 365–377.

50 G. Singh, H. Chan, A. Baskin, E. Gelman, N. Repnin, P. Král and R. Klajn, *Science*, 2014, **345**, 1149–1153.

51 G. Singh, H. Chan, T. Udayabhaskararao, E. Gelman, D. Peddis, A. Baskin, G. Leitus, P. Král and R. Klajn, *Faraday Discuss.*, 2015, **181**, 403–421.

52 S. Shinohara, D. Tanaka, K. Okamoto and K. Tamada, *Phys. Chem. Chem. Phys.*, 2015, **17**, 18606–18612.

53 A. Sánchez-Iglesias, M. Grzelczak, J. Pérez-Juste and L. M. Liz-Marzán, *Angew. Chem., Int. Ed.*, 2010, **49**, 9985–9989.

54 J. Y. Kim, S. Raja and F. Stellacci, *Small*, 2011, **7**, 2526–2532.

55 J. Y. Kim, S. J. Kwon, J.-B. Chang, C. A. Ross, T. A. Hatton and F. Stellacci, *Nano Lett.*, 2016, **16**, 1352–1358.

56 L. Scarabelli, M. Coronado-Puchau, J. J. Giner-Casares, J. Langer and L. M. Liz-Marzán, *ACS Nano*, 2014, **8**, 5833–5842.

57 A. B. Serrano-Montes, D. J. de Aberasturi, J. Langer, J. J. Giner-Casares, L. Scarabelli, A. Herrero and L. M. Liz-Marzán, *Langmuir*, 2015, **31**, 9205–9213.